Nuclear Inst. and Methods in Physics Research, A 992 (2021) 165048

Contents lists available at ScienceDirect

Nuclear Inst. and Methods in Physics Research, A

journal homepage: www.elsevier.com/locate/nima

Realization of the optimal beam dilution pattern of the FCC-hh ring using beating frequencies

Dániel Barna [a,b,*], Benedek Facskó [a], Anton Lechner [c], Elisabeth Renner [c]

[a] Wigner Research Centre for Physics, 1121 Budapest, Konkoly-Thege Miklós út 29-33, Hungary
[b] University of Miskolc, Faculty of Material Science and Engineering, Hungary
[c] CERN, Switzerland

ARTICLE INFO

Keywords:
FCC
Future Circular Collider
Beam dump
Beam extraction
Beam dilution

ABSTRACT

In order to avoid the damage of the dump target of the Future Circular Collider's proton ring, the beam will be swept over its surface using dilution kickers oscillating in the x/y planes with 90° phase difference, and an amplitude changing with time, thereby creating a spiral-like pattern. The natural time-dependence of the amplitude is the exponential decay of a damped oscillating circuit, which results in a decreasing pitch, and thereby increasing energy deposition density towards small radii. Compared to the optimal pattern with a flat energy density, this pattern requires a larger target size, larger total kicker strength or higher allowed energy density in the target material. We propose the realization of the optimal pattern using two beating frequencies. This method has the advantage of using the same, very simple circuitry as the baseline proposal: independent damped oscillator circuits (including the kicker magnets), which interfere only in their effect on the beam. This concept results in an 18% decrease of the maximum excursion of the pattern (i.e. target size), and 13% decrease of the total kicker power with respect to the baseline solution, at no extra cost. Besides the demonstration of the concept, a sensitivity analysis to the circuit parameters is presented.

1. Introduction

The Future Circular Collider (FCC) study [1] was launched in 2014 to identify the key challenges of the next-generation particle colliders after the Large Hadron Collider (LHC), propose technical solutions and establish baseline designs for the different machines covered by the study. One of these challenges is the handling of the unprecedented 8.3 GJ stored energy of the circulating beams in the proton–proton collider FCC-hh [1]. Table 1 compares the relevant parameters of the FCC-hh and LHC beams. Both beams must be extracted from the ring and absorbed in a dump target at the end of all collision cycles, or in case of any critical fault signal from the interlock system (safety beam abort). The beam extraction system is illustrated schematically in Fig. 1a for both the LHC and FCC-hh rings. The beam receives a small kick from a fast-switched (3 μs and 1 μs rise times for the LHC and FCC, respectively) extraction kicker magnet system (MKD), and starts to diverge from the nominal trajectory, entering into the high-field domain of the septum magnet, which then gives the final and large deviation to the beam out of the ring. In order to avoid that during the rise-time of the extraction kicker magnets some bunches are swept across the protection elements (not shown) and the physical wall of the septum magnet between its zero-field and high-field domains, the fill pattern of the ring contains beam-free intervals (1 and 4 for the LHC and FCC, respectively), called the "abort gaps". The extraction kicker magnets are normally triggered synchronously to the passage of the abort gap (synchronous beam dump).

Fault signals of the entire accelerator complex are classified by their severity, and require different actions. Their discussion is beyond the scope of this paper, see [2–4] for more details. These fault signals interrupt the beam interlock loop and typically trigger a beam abort with a reaction time of the extraction system of less than 3 turns, i.e. 1 ms, synchronized with the abort gap. Spurious, partial triggering of the MKD magnets is a critical fault that causes the beam to start oscillating within the ring. Since the fault is within the extraction system, a safety abort could physically be triggered much faster than in the general case mentioned above, with a reaction time which is less than the distance between the abort gaps. It is important to note that due to the highly modular design of the extraction kicker system, the impact of a single misfiring MKD module has been minimized to such a level that the immediate re-triggering of the entire extraction system (eventually out of synchrony with the abort gap, i.e. an asynchronous dump) is not needed. The miskicked beam would oscillate with a

* Corresponding author at: Wigner Research Centre for Physics, 1121 Budapest, Konkoly-Thege Miklós út 29-33, Hungary.
E-mail addresses: barna.daniel@wigner.hu (D. Barna), facsko.benedek@wigner.hu (B. Facskó), anton.lechner@cern.ch (A. Lechner), elisabeth.renner@cern.ch (E. Renner).
URL: http://wigner.hu/~barna (D. Barna).

https://doi.org/10.1016/j.nima.2021.165048
Received 4 September 2020; Received in revised form 14 December 2020; Accepted 11 January 2021
Available online 14 January 2021

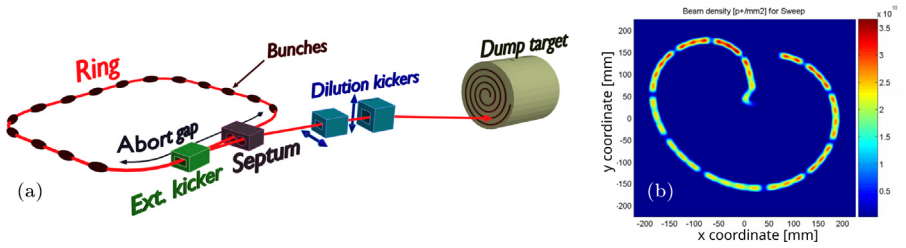

Fig. 1. (a) Schematic illustration of the beam extraction system (in reality, the LHC uses a two-plane extraction scheme where the beam is deflected horizontally by the kickers, and vertically by the Lambertson septa; in the FCC both would deflect the beam vertically). (b) Dump pattern of the LHC.

displacement of about 1.5σ around the nominal trajectory, which can be accommodated by the ring, and the subsequent beam abort would be synchronized with the next abort gap. These measures minimize the probability of an asynchronous dump. Nevertheless, this scenario cannot be excluded completely at this stage of the design, and has to be dealt with. This can happen in case of the spurious triggering of several or all MKD units, which can be due to the failures of the trigger synchronization unit, or the trigger fan out, which distributes the trigger to the MKD generators.

Dumping the beam poses a challenge already at the LHC with an almost 23 times lower stored energy: there exists no technical solution today to safely absorb this energy impinging into a single spot, and the beam therefore needs to be distributed over the surface of a large target block made of graphite or carbon-reinforced composite (CfC) materials, which are suitable for this purpose since they combine a relatively low density with a high thermal shock resistance and a high melting point.

The high-energy protons impacting on the dump core create a hadronic cascade via inelastic hadron–nucleus collisions, accompanied by an electromagnetic shower component due to the decay of neutral pions into energetic gammas. A significant fraction of the energy released by the beam in the dump is eventually dissipated by the electromagnetic component. The maximum energy deposition density and hence the peak temperature in the dump critically depend on the overlap of transverse shower tails of different proton bunches swept across the dump surface. When designing the sweep pattern, it is important to study both the separation of bunches along the sweep path and the radial separation of different spiral branches. Even for large radial branch separations of several centimetres, the overlap of shower tails is not negligible and has to be taken into account in the optimization of the pattern.

The dump pattern of the LHC is shown in Fig. 1b. A similar system is planned for the FCC-hh ring, but due to the longer bunch train (10400 bunches instead of the 2808 in the LHC, arriving at the same intervals of 25 ns) and the higher stored energy, the extraction system and the dilution pattern of the beam is more complex [5]. The natural choice for the pattern is a spiral, which can be realized by two sets of oscillating kicker magnets, deflecting the beam in the horizontal and vertical directions, respectively (Fig. 1a), with a 90° phase difference between them, and an amplitude changing with time. In order to maintain the inductive voltage of the kicker magnets, and the requirements on the power supplies within limits, the dilution kicker magnet system is planned to be modular, consisting of several tens of independent circuits containing a single magnet and its driving circuitry [1,2,6]. As described before, this arrangement also contributes to the mitigation of the consequences of hardware failure (no or erratic triggering), by reducing the effect of a single failing module.

Although different dilution patterns could be constructed to efficiently distribute the beam on the dump target with an allowed maximum energy deposition density, the feasibility of the necessary hardware is a major limit on one's creativity. In particular, using a fixed-frequency oscillation of the magnetic field seems to be by far the most realistic choice, and therefore in the following we will not address any dilution patterns which would require time-variant frequencies or any more complex waveforms. These considerations lead to a spiral pattern with fixed frequency, where the excursions of the pattern (x, y) in the two planes can be described as

Table 1
Parameters of the LHC and FCC-hh beams, relevant for the dump systems [1].

Parameter	LHC	FCC-hh	Unit
Stored energy per beam	0.35	8.3	GJ
Number of stored bunches	2808	10400	
Bunch-to-bunch spacing	25	25	ns
Revolution time (max. possible bunch train length)	90	326	μs
Dump beamline length	0.9	2.5	km

$$x = R(t)\sin(\omega t)H(t) \tag{1}$$

$$y = R(t)\sin(\omega[t-\pi/2\omega])H(t-\pi/2\omega) \tag{2}$$

where t is time, $R(t)$ is the time-dependent envelope of the kicker magnets' waveform, ω is the angular frequency of their oscillating field, and H is Heaviside's function describing the absence of any deflection before the trigger at $t = 0$. The peripheral progression velocity of this pattern decreases linearly with radius, and if the average bunch density is to be kept constant for the optimal distribution, the radial progression velocity $\mathrm{d}R(t)/\mathrm{d}t$ needs to increase linearly with $1/R$, resulting in the formulae

$$R_{\mathrm{o}}(t) = \sqrt{\frac{t}{\delta t}\frac{S_0}{\pi} + R_{\mathrm{min}}^2} \tag{3}$$

$$R_{\mathrm{i}}(t) = \sqrt{\frac{T-t}{\delta t}\frac{S_0}{\pi} + R_{\mathrm{min}}^2} \tag{4}$$

where δt is the bunch-to-bunch spacing, T is the length (in time) of the whole bunch train, S_0 is the average area necessary for a single bunch to stay below the damage threshold of the material, and $R_{\mathrm{min}} = d/\omega$ is the minimum radius of the pattern, determined from the frequency ω of the magnet circuit, and the minimum required spatial bunch separation d on the target. The subscripts o and i refer to an outward-running or inward-running pattern, respectively. Their difference will be discussed later. Even though this approach is oversimplified (the real energy deposition density must be calculated by the superposition of single-bunch energy deposition profiles), it nicely illustrates that for the optimal pattern the envelope function $R(t)$ needs to be concave. Unfortunately, the exponential envelope of the most natural implementation, a damped RLC circuit is convex, leading to a slow progression of the pattern in both the radial and peripheral directions, and thereby to an increasing energy distribution density towards small radii. This would in turn call for a larger dump target, and larger deviations by the dilution kickers (or longer tunnel length), in order to keep the maximum energy density in the allowed range.

For an outward-running spiral, the dilution kicker system does not require any pre-triggering; the pattern would never cross itself. The amplitude of the pattern (i.e. the total deflection by the dilution kicker magnets) is monotonically increasing with time, in contrast to the decreasing amplitude of the oscillating field of the individual kicker magnets, when damped oscillating circuits are used. Even though this scheme could be realized by the method described later in this

manuscript, it is difficult and ineffective, and will therefore not be treated further in this article. For an inward-running spiral pattern, the kicker magnets in one of the two planes must be pre-triggered, so that their magnetic field reaches its maximum by the time the first bunch arrives. The pattern then progresses by spiralling inwards. Pre-triggering is not possible in the case of an immediate asynchronous dump, resulting in a self-crossing pattern and the associated increased energy deposition density. Another problem of the asynchronous dump is the appearance of a "hot spot" in the energy deposition density map (see Fig. 8). This is due to the magnetic field of the kickers in one plane reaching its extremum and having a zero time-derivative, right before the trigger in the other plane, if the sharp 90°-offset triggering scheme described by Eq. (2) is used. This leads to the overlap of several subsequent bunches. It must be noted that in the LHC the circuits of both planes are triggered simultaneously, but one of them is modified to exhibit a longer initial risetime, leading to its 90° delay [7]. This configuration would reduce the maximum energy density at the above mentioned hot spot in case of an asynchronous dump. On the other hand, the modifications of the circuits of one plane can have unwanted side-effects on the precise shape of the waveform, and thereby on the long, carefully tuned and delicate 2D pattern. This has not been studied in detail yet.

A further requirement on the dump system is that it should safely tolerate a failure rate of as much as 10% of the dilution kickers (i.e. only 90% of them being triggered) [1,2]. The value of 10% has been chosen somewhat arbitrarily giving a failure tolerance margin in the operation of the machine before intervention is unavoidable.

2. Synthesis of the ideal pattern by beating frequencies

A well known method to realize a desired waveform is to synthesize it as the weighted sum of a series of harmonic components (Fourier synthesis). Since the building blocks of the baseline proposal for the hardware are RLC circuits (where the inductive component is practically the magnet itself, and the damping is due to all the losses of the circuit), it seems natural to ask whether the purely harmonic components of the Fourier synthesis could be replaced by damped sinusoidal functions, and for the sake of simplicity of the following analysis, to only use a few different frequencies — at the extreme case only two. This case is more properly called "beating frequencies". Since the dilution kicker system is anyway planned to be modular, the beating frequencies method could be realized with the same hardware as in the baseline proposal. The different units only need to be classified into two different frequency classes, and would remain otherwise unchanged, and uncoupled from each other. It is only their effect on the beam, which interferes and produces the desired pattern.

In the following the problem will be discussed in terms of excursions of the pattern from the origin measured at the target. This decouples the problem from kicker magnet and beamline parameters, which can then be defined later, as a function of one-another. The excursion of the pattern is parameterized as

$$x(t) = A_1 \exp\left(-\frac{t}{\tau}\right) \sin\left(2\pi[f-\Delta f]t\right) H(t) + A_2 \exp\left(-\frac{t-\Delta t}{\tau}\right) \sin\left(2\pi f[t-\Delta t]\right) H(t-\Delta t) \quad (5)$$

in the horizontal plane, where A_1 and A_2 are the amplitudes of the two components measured in metres, $\tau = Q/2\pi f$ and f are the time constant and frequency of the damped circuit, respectively, Q is the quality factor of the resonator circuit, Δf is the difference between the two frequencies, Δt is the delay (i.e. an initial phase difference) between the two components, which is calculated from the easier-to-understand phase difference $\Delta\phi$ as $\Delta t = \Delta\phi/2\pi f$, and Heaviside's function H is again describing the absence of any deflection before the trigger. The pattern's excursion in the other plane, $y(t)$ was defined by the same formula as $x(t)$, but triggered at a 90° phase delay calculated from the weighted average of the two frequencies:

$$y(t) = x(t - \hat{T}/4) \quad (6)$$

$$\hat{T} = \frac{A_1 + A_2}{A_1(f-\Delta f) + A_2 f} \quad (7)$$

As is visible from the above equations, the same two frequencies are used in both planes. Different frequencies would lead to a less even energy distribution, and if a large enough phase slip is reached between the two planes during the long bunch train, the pattern would be similar to a self-crossing Lissajous curve.

For the frequency f the highest feasible value is preferred, giving the largest bunch-to-bunch separation on target. In the following analysis $f = 50$ kHz was used, which is a compromise between the total number of magnets and generators (cost) and the goal to limit the maximum voltage (to increase the reliability of the system). For example, the system voltage is $V = 2\pi f N A l_m F B = 20$ kV for magnets with a length of $l_m = 1.5$ m, aperture (in both planes) of $A = 35$ mm, magnetic field of $B = 1$ T, frequency $f = 50$ kHz, and a factor $F = 1.2$ accounting for the stray inductance with respect to the hard-edge model. Higher frequency could either be reached using shorter (more) magnets, or higher voltage. More magnets mean more circuits and thereby an increased cost, and more gaps between the magnets, leading to a smaller average field. Restricting Δf to be positive, the frequency of the other component will remain below this limit as well. For the quality factor the value $Q = 200$ was chosen as a realistic estimate based on the experience with similar hardware in the past.

The FCC dump core is assumed to be composed of different graphite segments similarly to the dump configuration presently used in the LHC. The central part of the core, where the particle showers reach their maximum, is assumed to be filled with graphite of low density (1.0 g/cm^3) in order to reduce the maximum energy deposition density and hence the maximum temperature induced by the FCC bunches (see Fig. 2 and the annotations in Fig. 3a). This low-density segment is assumed to be complemented by higher-density graphite blocks (1.8 g/cm^3) at both the up- and downstream ends in order to enhance the absorbing capabilities of the dump and therefore reduce the overall dump length. Here we assume that the upstream higher-density segment is 1.5 m long, followed by a 4.5 m long lower density segment. The total dump length needs to be of the order of 10 m. Fig. 3a shows the maximum energy deposition density due to a single bunch as a function of penetration depth into the dump target, as obtained by a FLUKA [8,9] simulation. Fig. 3b shows the radial energy deposition density profile of a single bunch impinging at the origin, at a depth of 375 cm, where the maximum energy deposition density was found to be the highest for the typical sweep patterns.

Fig. 3c shows the 2D transverse energy deposition density map for a single bunch impinging at the origin, on a 1×1 mm grid. This was obtained by integrating the fitted radial function (shown in Fig. 3b) within each bin. The energy density map of a complete sweep pattern must then be calculated by the superposition of such maps, shifted by the impact positions (measured in integer number of bins) of the bunches. This method is, however, insensitive to the relative position of a bunch impact within a bin. In order to refine the sensitivity without significantly increasing the computing time, the following approach was used. Nine such single-bunch transverse profile histograms were pre-calculated as described before, with the impact position of the bunch being scanned over 3×3 positions within the bin, at $x, y = (-1/3, 0, 1/3) \times b$ with respect to the bin centre, where b is the binsize. For each bunch of the beam, its relative impact position within a bin was determined and then used to choose one of these nine histograms with the closest relative impact position. These histograms were shifted by the appropriate number of bins and superimposed to get the energy deposition map of the entire beam.

A large pattern requires a large dump target, and powerful (or numerous) dilution kickers and/or a long tunnel. High maximum energy deposition density requires more sophisticated target material and structure. There is a trade-off between the two goals of having a small pattern and low maximum energy deposition density. This trade-off is partial, because even a large pattern can have high maximum energy

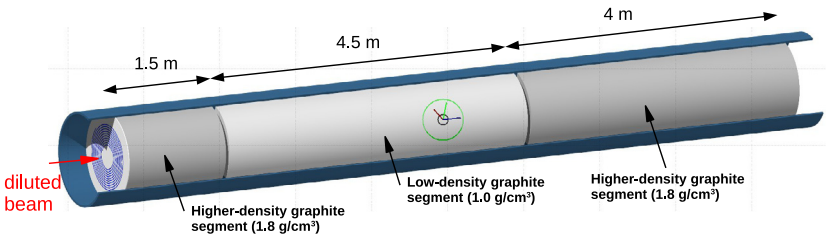

Fig. 2. Geometry model of the FCC beam dump used in this study.

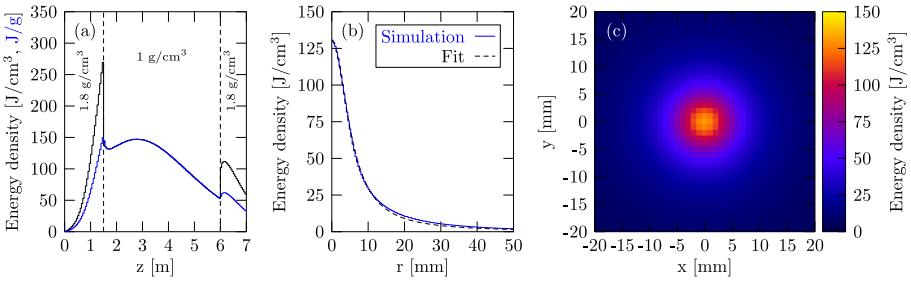

Fig. 3. (a) Longitudinal profile of the maximum energy deposition density of a single bunch as a function of penetration depth, plotted as energy deposited per unit volume (J/cm^3, black) or unit mass (J/g, blue), evaluated over the transverse plane. The dashed vertical lines indicate the boundaries between three domains of the graphite target with densities 1.8 g/cm^3, 1 g/cm^3 and 1.8 g/cm^3. (b) Simulated and fitted radial energy deposition density profile of a single bunch at a depth of 375 cm. The fitted function is $E = 38.91/\left[r^2 + 0.2988\right]$, where E is the energy deposition density measured in J/cm^3, and r is the radial distance measured from the origin in centimetres. (c) Two-dimensional energy deposition density map of a single bunch impinging at the origin. (For interpretation of the references to colour in this figure legend, the reader is referred to the web version of this article.)

deposition density if the pattern is not optimized, and has an uneven energy distribution. In order to take into account both goals, a penalty function was defined as the weighted sum of the maximum excursion of the pattern, S, and the maximum energy deposition density of the superimposed map, $E_{\max}$:

$$P = w_e \frac{E_{\max}}{E_0} + w_s \frac{S}{S_0} \tag{8}$$

Here, w_e and w_s are the weights associated with the energy- and size-terms of the penalty function, giving different importances to the two goals. The purpose of the two scaling factors S_0 and E_0 is to make the two terms dimensionless, and to bring their values to the same order of magnitude. S_0 was chosen to be 0.6 m, which is a typical size of the patterns, determined during the development of the algorithm empirically. E_0 = 5 kJ/cm^3 is an energy scale factor, defined as the maximum energy density we allow in the target material. The choice of its value was motivated by previous material robustness tests with 440 GeV proton beams at CERN's HiRadMat facility [10,11], where energy deposition densities of ≈3.4 kJ/g have been achieved in Graphite and CfC targets (≈1.8 g/cm^3). No material failure has been observed in these irradiation experiments. We assume that a similar energy deposition per unit mass is also acceptable for the considered low density segment (1.0 g/cm^3) of the FCC dump core. For rare failure scenarios, like the asynchronous beam dumps, higher energy densities up to 4–5 kJ/g could be allowed. It cannot be excluded that local damage occurs inside the dump for such energy densities, but the dump is expected to remain functional. More irradiation experiments, material characterization studies and thermo-structural simulations are needed to better quantify the acceptable load conditions for the FCC dump. The beam brightness achieved so far in the HiRadMat facility did not permit to probe the damage limit of Graphite and CfC absorbers. It is expected that up to 80% higher bunch intensities can be reached in the HL-LHC era, which will offer the opportunity to test the response of these materials for peak loads higher than 5 kJ/g. Depending on the outcome of these future experiments, the allowed energy density might require an adjustment, but this does not affect the general ideas presented in this paper.

A simplex minimum-finding algorithm was used to find the minimum of the penalty function as a function of the free parameters A_1, A_2, Δf and Δt. The optimization was made with different weights, keeping their sum $w_e + w_w = 1$ constant.

The fill pattern of the ring is complex, containing several gaps (due to the filling scheme, or the abort gaps). Interplay of these gaps with each other or the binning structure would cause a more unsmooth behaviour of the penalty function. Therefore during the optimization, a continuous fill pattern was used, with bunches spaced at every 25 ns for a length of 326 μs. This choice gives an upper estimate of the maximum energy deposition density.

3. Results and discussion

Fig. 4 shows the maximum energy density and the maximum excursion of the optimized dilution pattern, as a function of the ratio of the two weights. As is visible, when increasing the ratio w_e/w_s, the algorithm gives more weight to the maximum energy density in the penalty function and therefore tries to decrease it more aggressively, at the cost of an increased pattern radius. This approach leaves a decision possibility for the designers at a later stage, when the concept is more developed, and more is known about the hardware (material and equipment price, damage threshold of the target material, etc.). The exact values of the scaling factors S_0 and E_0 are not relevant, their change would simply result in the same optimized hardware parameters at a different value of the otherwise irrelevant ratio w_e/w_s.

Fig. 5 shows the optimized values of the parameters in Eq. (5) as a function of the weight ratio w_e/w_s. The last three points in Fig. 5b, and the last point in Fig. 5c seem to break the smooth trend shown by the remaining points. However, the scattering of these points is small compared to the value of these parameters. It is due to the reduced sensitivity and the unsmooth behaviour of the penalty function in response to these parameters. These scattering points have no significance.

As is visible in Fig. 5a, the values of A_1 and A_2 fall close, meaning that the number of kickers with similar strengths is balanced between the two frequency classes. The sum of these amplitudes (dashed line), i.e. the total power of all kicker units, is larger than the maximum excursion of the pattern (solid black line, replotted from Fig. 4b). This is due to the fact that initially, when the inward-running spiral is at its maximum excursion, the two frequencies are in a partially constructive

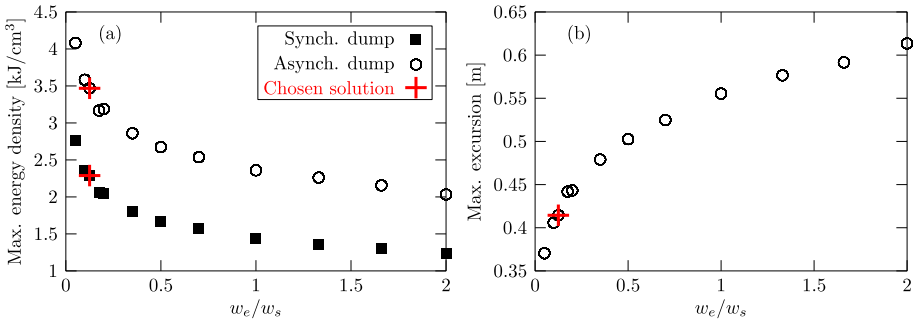

Fig. 4. (a) Maximum energy density, and (b) maximum excursion of the dilution pattern, as a function of the weight of the energy- and size-terms of the penalty function.

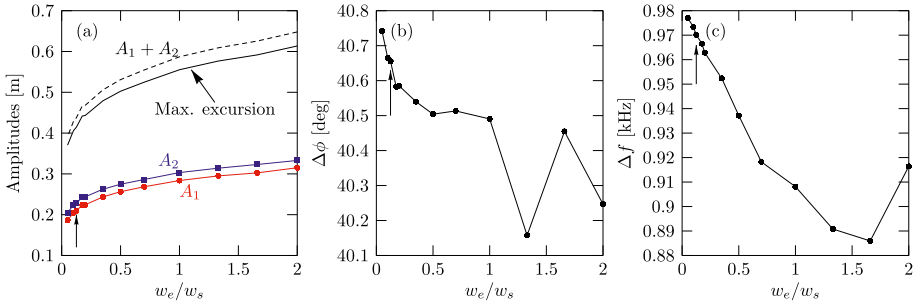

Fig. 5. Values of the optimized parameters as the function of the w_e/w_s weight ratio: (a) amplitudes of the two components with different frequencies, their sum, and the total excursion of the pattern resulting from the beating of the two frequencies; (b,c) phase offset and frequency difference between the two components acting in the same plane. The arrows indicate the chosen solution.

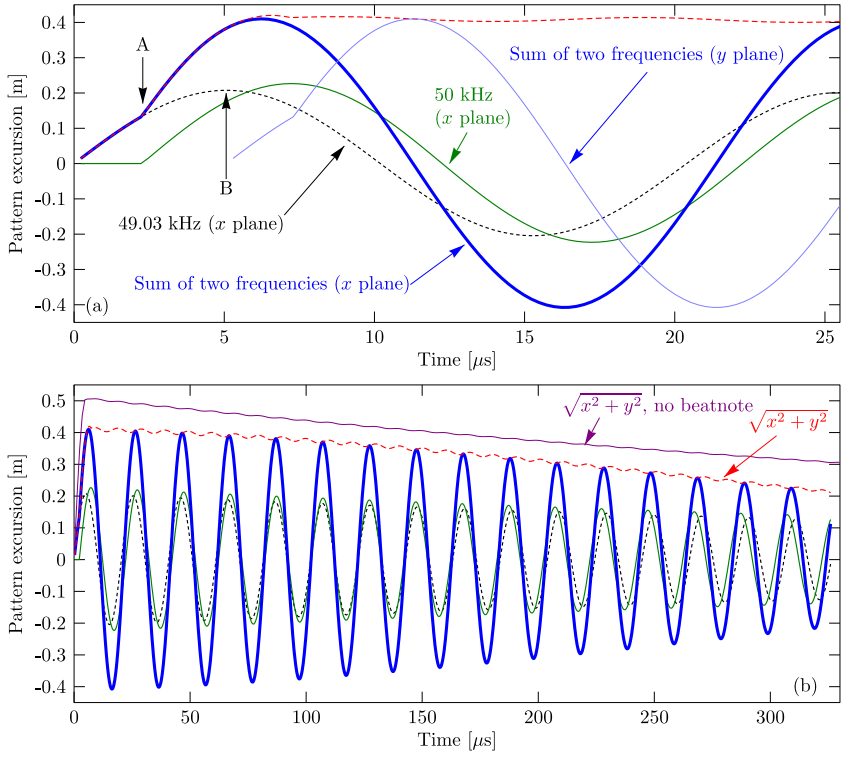

Fig. 6. Waveforms of the dilution sweep patterns in the x and y planes, and total excursion of the pattern from the origin for the weight ratio w_e/w_s = 0.125: (a) during the first 25 μs, (b) during the full length of the beam. Solid green and dashed black lines: waveforms of the two frequency components of the optimized scheme in the x plane (both plots). Solid thick blue line: sum of the two frequency components (complete waveform) of the optimized scheme in the x plane (both plots). Solid thin blue line: the delayed, complete waveform of the optimized scheme in the y plane [plot (a) only]. Dashed red line: radial excursion of the optimized dilution pattern (both plots). Solid magenta line: radial excursion of the unoptimized, exponential dilution pattern with the same maximum energy deposition density [plot (b) only]. The arrows marked by "A" and "B" indicate the trigger of the second frequency component in the x plane, and the trigger of the first frequency component in the y plane. The same marks are also shown in Fig. 8. (For interpretation of the references to colour in this figure legend, the reader is referred to the web version of this article.)

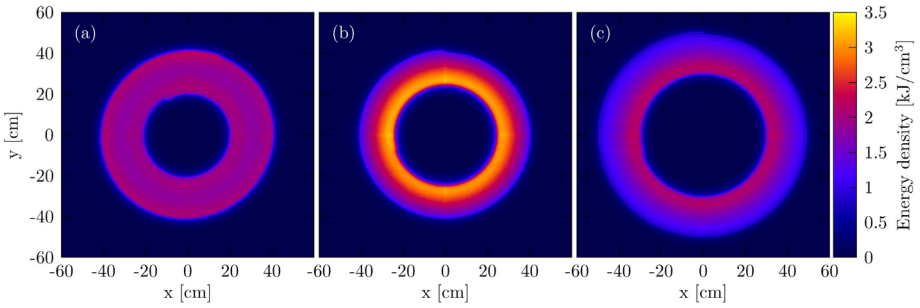

Fig. 7. Energy density map of three patterns in case of a synchronous dump: (a) the optimized pattern using beating frequencies, (b) a simple, exponentially damping spiral with the same maximum excursion as for the optimized pattern, and (c) an exponentially damping spiral with the same maximum energy density as for the optimized pattern. (For interpretation of the references to colour in this figure legend, the reader is referred to the web version of this article.)

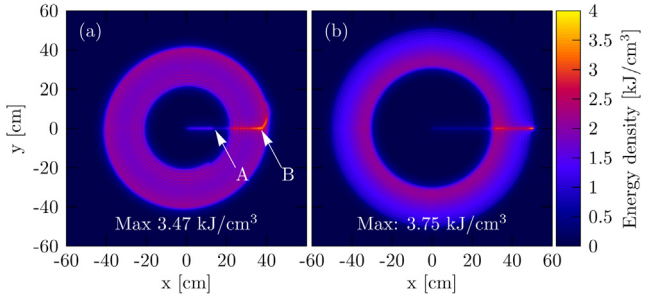

Fig. 8. Dilution patterns in case of an asynchronous dump: (a) optimized pattern, (b) exponentially damped pattern (same parameters as in Fig. 7c). The arrows marked by "A" and "B" indicate the trigger of the second frequency component in the x plane, and the trigger of the first frequency component in the y plane. The same marks are also shown in Fig. 6. (For interpretation of the references to colour in this figure legend, the reader is referred to the web version of this article.)

Table 2
Values of the optimized parameters at the chosen weight ratio of w_e/w_w=0.125.

Parameter	Value	Unit
E_{max}	2.289	kJ/cm³
S	0.414	m
A_1	0.209	m
A_2	0.228	m
$\Delta\phi$	40.66	degree
Δf	0.97	kHz

interference only, their phase difference being around 40.5° (Fig. 5b). Since $\Delta\phi$ and Δf are positive, the higher-frequency component is triggered later, and will "catch up" with the other component with time, getting into a fully constructive interference condition, as illustrated in Fig. 6. After this the two frequencies will start to run out of phase again, and lose fully constructive interference. This results in the concave envelope of the superposition of the two components, shown by the red line in Fig. 6, even though their individual envelopes are convex (exponential).

For Fig. 6 and in the following illustrations the optimized solution at $w_e/w_s = 0.125$ was chosen, which gives a good and realistic compromise between maximum energy density and dump target size. The values of the resulting parameters are shown in Table 2. Fig. 7a shows the energy deposition density map of the optimized pattern, in case of a synchronous dump. Fig. 7b shows the same map for an exponentially damped spiral pattern with the same size, which has a 40% higher maximum energy deposition density. Fig. 7c shows an exponentially damped spiral pattern with the same maximum energy as that of the optimal pattern. With respect to this pattern, the optimized pattern has 18% less maximum excursion, and 13% less total kicker power.

A further benefit of the proposed method is the reduction of the high energy density at the hot spot for an asynchronous dump, which comes as a bonus. The first trigger of the kickers in the y plane (marked with "B" in Figs. 6 and 8a) is at an approximately 90° phase delay with respect to the first component of the waveform in the x plane. Since now the waveforms are not purely harmonic but have two components with a certain delay, the maximum of the kicker waveform in the x plane is not in coincidence with the first trigger in the y plane, but at a later time. That is, the progression of the pattern does not come to a full stop at any time. Fig. 8 shows the energy deposition density maps for the optimized and exponentially damped patterns, in case of an asynchronous dump. The optimized pattern has a hot-spot energy density reduction of about 8%.

The dilution pattern is created by the interplay between two simple oscillatory components with fine-tuned frequency differences, and relative delays (the latter being between the two different frequency-components acting in the same plane, as well as between the waveforms of the two planes). In practice, each of the two frequency components of the beating waveform of one plane is realized as several individual magnet modules. Uncertainties of the parameters of these magnet modules can destroy the fine-tuned interference, and finally lead to the distortion of the ideal pattern. In order to study this effect, each of the two frequency components of a waveform, acting in any of the two transverse planes, was decomposed into multiple parts:

$$x(t) = \sum_{i=1}^{N_1} A_1^{(i)} \exp\left(-\frac{t+\delta t^{(i)}}{\tau^{(i)}}\right) \sin\left(2\pi[f^{(i)} - \Delta f][t+\delta t^{(i)}]\right) H(t+\delta t^{(i)}) + \sum_{j=1}^{N_2} A_2^{(j)} \exp\left(-\frac{t+\delta t^{(j)} - \Delta t}{\tau^{(j)}}\right) \sin\left(2\pi f^{(j)}[t+\delta t^{(j)} - \Delta t]\right) \times H(t+\delta t^{(j)} - \Delta t) \quad (9)$$

and similarly for the waveform in the y plane. N_1 and N_2 is the assumed number of modules of the two frequency components. The parameters bearing the upper indices in parentheses, $A_1^{(i)}$, $A_2^{(j)}$, $\tau^{(i,j)}$, $f^{(i,j)}$, and the time jitter $\delta t^{(i,j)}$ were randomly generated around their respective ideal values A_1/N_1, A_2/N_2, τ, f and 0, according to a normal distribution with standard deviations given in Table 3. These values were determined based on past experience with the given type of hardware. The number of units was chosen to be $N_1 = 19$, $N_2 = 21$, since these values seem to be realistic based on a general beamline optimization study running in parallel to the current work, taking into account realistic hardware parameters (magnetic field, magnetic length, aperture, tunnel length, etc.). The ratio of the two integer numbers N_1/N_2 is chosen to be close to the ratio of the amplitudes A_1/A_2, ensuring that the magnetic field of the individual magnets are roughly equal.

A set of 10 000 patterns was generated with randomly chosen hardware parameters. Fig. 9a shows the distributions of the maximum energy densities for a synchronous and asynchronous dump. Since the parameters were optimized for a synchronous dump, all perturbations result in a worse scenario in this case, i.e. higher maximum

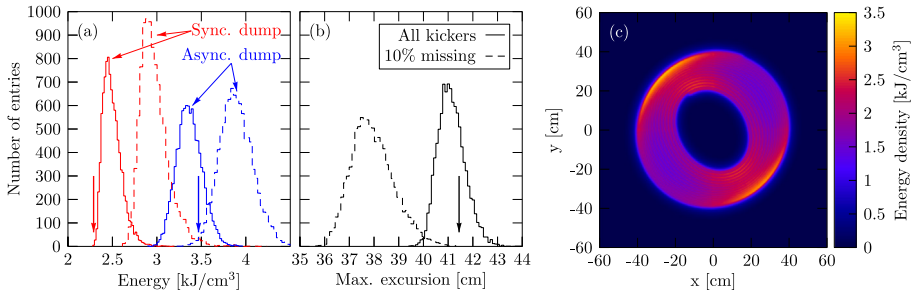

Fig. 9. Distribution of (a) the maximum energy densities for a synchronous and asynchronous dump, and (b) the maximum excursion of the patterns due to the uncertainty of the hardware parameters. The dashed lines show the case when 10% of the kickers fails. The arrows indicate the corresponding values for the ideal, unperturbed case. (c) A particular pattern with perturbed parameters. (For interpretation of the references to colour in this figure legend, the reader is referred to the web version of this article.)

Table 3
Assumed uncertainties of the hardware parameters.

Parameter	standard deviation
Frequency (f)	±0.2%
Amplitude (A)	±2%
Time constant (τ)	±1%
Time jitter (δt)	± 250 ns

energy density. The same statement does not hold for the case of the asynchronous dump. For each of the parameter sets, the maximum energy density stays below the maximum allowed energy density in the target material (5 kJ/cm^3), although for the worst error case, an asynchronous dump with 10% of the kickers (randomly chosen from the two frequency classes) failing, the distribution extends significantly between 4–5 kJ/cm^3. A more reliable value of the maximum allowed energy will later be estimated based on dedicated experiments. The study must then be repeated, possibly choosing a different w_e/w_s ratio in Fig. 5 if needed. Fig. 9b shows the distribution of the maximum excursion of the patterns, for all kickers on, or 10% of the kickers failing. The distributions extend over a range of few centimetres only, and therefore no extra physical margin is required for the dump target due to the parameter uncertainties beyond what would be determined for the unperturbed pattern. Fig. 9c shows a particular pattern with a relatively high maximum energy density chosen from the simulated set.

4. Summary

Handling and safely disposing the extremely large energy stored in the circulating beams of the planned Future Circular Collider poses a major challenge for the design of both the extraction system and the dump target. There exists no material today, which could survive the impact of the beam into a single spot. Therefore a set of magnets called "dilution kickers" with oscillating fields in the two transverse planes is foreseen to distribute the beam over an extended target. With an amplitude decreasing with time, and a 90° phase difference between them, the resulting pattern is an inward-running spiral. However, the exponential attenuation of the amplitude of the trivial hardware choice, a lossy RLC magnetic circuit, leads to an increasing energy deposition density towards small radii. As a consequence, the pattern (and thereby both the target size, and the kickers' strength) needs to be larger than for a spiral with a flat energy deposition density. This work has presented a new concept of using several magnet modules grouped into two different frequency classes, so that the interference of their effect on the beam produces an optimized pattern with a flat energy deposition density. An attractive feature of this concept is that it can be realized with the very same simple hardware as that used in the baseline design, namely a set of independent RLC circuits in which the inductive component is the magnet itself. Application of this concept could decrease the dump target size by 18%, and the total strength of the kicker magnets by 13%. A bonus feature of this concept is the 8% reduction of the high energy deposition density at the "hot spot" associated with asynchronous dumps, due to the absence of coincidence of the trigger in the y plane with the maximum of the waveform in the x plane. Scattered values of the hardware parameters can destroy the fine-tuned interference between the individual modules. This effect was estimated and shown to stay within acceptable limits.

CRediT authorship contribution statement

Dániel Barna: Conceptualization, Methodology, Software, Investigation, Visualization, Supervision, Writing - original draft, Writing - review & editing. **Benedek Facskó:** Conceptualization, Methodology, Software, Investigation, Visualization, Validation, Writing - original draft, Writing - review & editing. **Anton Lechner:** Software, Investigation, Visualization, Writing - original draft, Writing - review & editing. **Elisabeth Renner:** Investigation, Writing - original draft, Writing - review & editing.

Declaration of competing interest

The authors declare that they have no known competing financial interests or personal relationships that could have appeared to influence the work reported in this paper.

Acknowledgements

The research presented in this paper was supported by the Hungarian National Research, Development and Innovation Office under grant no. K124945 (at Wigner Research Centre for Physics), and the Thematic Excellence Program funded by the Ministry of Innovation and Technology of Hungary under grant nos. NKFIH-846-8/2019 and TKP-17-1/PALY-2020 (at the University of Miskolc). D.B. was supported by the János Bolyai Scholarship of the Hungarian Academy of Sciences. The authors are grateful to Mike Barnes and Thomas Kramer for their useful input and suggestion during this work.

References

[1] M. Benedikt, et al., FCC-hh: The hadron collider. Future circular collider conceptual design report volume 3, Eur. Phys. J. Spec. Top. 228 (2019) 755–1107, http://dx.doi.org/10.1140/epjst/e2019-900087-0.

[2] E. Renner, Machine Protection of the Future Circular Hadron Collider FCC-hh: Injection and Extraction (Master's thesis), Vienna University of Technology, Vienna, 2018, URL: https://cds.cern.ch/record/2648770/files/CERN-THESIS-2018-261.pdf.

[3] Y. Nie, R. Schmidt, J. Uythoven, C. Wiesner, D. Wollmann, M. Zerlauth, Concept of beam-related machine protection for the future circular collider, JACOW Publishing, Geneva, Switzerland, 2019, pp. 4085–4088, http://dx.doi.org/10.18429/JACoW-IPAC2019-THPRB113, URL: http://accelconf.web.cern.ch/ipac2019/doi/JACoW-IPAC2019-THPRB113.html.

[4] R. Schmidt, R. Assmann, E. Carlier, B. Dehning, R. Denz, B. Goddard, E.B. Holzer, V. Kain, B. Puccio, B. Todd, J. Uythoven, J. Wenninger, M. Zerlauth, Protection of the CERN large hadron collider, New J. Phys. 8 (2006) 290, URL: https://iopscience.iop.org/article/10.1088/1367-2630/8/11/290.

[5] W. Bartmann, M. Atanasov, M.J. Barnes, J. Borburgh, F. Burkart, B. Goddard, T. Kramer, A. Lechner, A. Sanz Ull, R. Schmidt, L.S. Stoel, R. Ostojic, J. Rodziewicz, P. van Trappen, D. Barna, Dump system concepts for the Future Circular Collider, Phys. Rev. Accel. Beams 20 (2017) 031001, http://dx.doi.org/10.1103/PhysRevAccelBeams.20.031001, URL: https://journals.aps.org/prab/abstract/10.1103/PhysRevAccelBeams.20.031001.

[6] M.J. Barnes, W. Bartmann, F. Burkart, L. Ducimetière, B. Goddard, T. Kramer, V. Senaj, T. Stadlbauer, D. Woog, D. Barna, L.M. Redondo, A. Kandratsyeu, Future circular collider injection and extraction kicker topologies and solid state generators, Phys. Rev. Accel. Beams 22 (7) (2019) 071001, http://dx.doi.org/10.1103/PhysRevAccelBeams.22.071001, URL: https://link.aps.org/doi/10.1103/PhysRevAccelBeams.22.071001, Publisher: American Physical Society.

[7] L. Ducimetière, LHC Beam Dump System, Kicker magnets and generators, 2008, https://indico.cern.ch/event/464373/contributions/1970395/attachments/1195579/1737262/LBDS_audit_LD_km_2008.pdf.

[8] G. Battistoni, T. Böhlen, F. Cerutti, P.W. Chin, L.S. Esposito, A. Fassó, A. Ferrari, A. Lechner, A. Empl, A. Mairani, A. Mereghetti, P.G. Ortega, J. Ranft, S. Roesler, P.R. Sala, V. Vlachoudis, G. Smirnov, Overview of the FLUKA code, Ann. Nucl. Energy 82 (2015) 10–18, URL: http://dx.doi.org/10.1016/j.anucene.2014.11.007.

[9] T. Böhlen, F. Cerutti, P.W. Chin, A. Fassó, A. Ferrari, P.G. Ortega, A. Mairani, P.R. Sala, G. Smirnov, V. Vlachoudis, The FLUKA code: Developments and challenges for high energy and medical applications, Nucl. Data Sheets 120 (2014) 211–214, URL: http://dx.doi.org/10.1016/j.nds.2014.07.049.

[10] F. Nuiry, M. Calviani, M. Bergeret, S. Pianese, M. Butcher, L. Grec, A. Lechner, M.I. Frankl, F.L. Maciariello, T. Pichon, 3d carbon/carbon composites for beam intercepting devices at CERN, Mater. Design Process. Commun. 1 (2019) e33, URL: https://doi.org/10.1002/mdp2.33.

[11] F.-X. Nuiry, et al., Low-z carbon based material testing through direct impact of high energy CERN Super Proton Synchrotron beam (HiRadMat), 2020, in preparation.